Upconversion Luminescence in Er^{3+}-Doped $RbGd_2Cl_7$ and $RbGd_2Br_7$

Toni Riedener, Karl Krämer, and Hans U. Güdel*

Institut für anorganische Chemie, Universität Bern, Freiestrasse 3, 3000 Bern 9, Switzerland

Received January 18, 1995[⊗]

Er^{3+}-doped $RbGd_2Cl_7$ and $RbGd_2Br_7$ have been synthesized and grown as crystals using the Bridgman technique. Crystal absorption, upconversion luminescence, and Raman spectra are presented. Efficient infrared to visible upconversion is observed in both compounds at all temperatures between 10 and 295 K. Under $^4I_{9/2}$ excitation around 800 nm both compounds show similar upconversion spectra, whereas their behavior is distinctly different for $^4I_{11/2}$ excitation around 980 nm. The green light of the chloride originates from $^4S_{3/2}$ luminescence, whereas the bromide has a pure $^4F_{7/2}$ luminescence in the blue. This is due to the difference in the highest-energy vibration which is 264 and 180 cm^{-1} for the chloride and bromide, respectively. Estimates of radiative and nonradiative rate constants are made for the various processes depopulating the $^4F_{7/2}$ state. Measured oscillator strengths of f–f transitions are compared with those determined from a Judd–Ofelt calculation. It is found that the $^4F_{7/2} \rightarrow {}^4I_{15/2}$ is a potential laser transition in bromide lattices.

1. Introduction

The phenomenon of upconversion, i.e. photoexcitation at a certain wavelength followed by luminescence at a shorter wavelength, is quite common in compounds containing lanthanide ions.[1] In contrast, very few reports on upconversion processes in transition metal ion systems have appeared so far.[2,3] Most Er^{3+} compounds show visible luminescence when excited into $^4I_{11/2}$ (near 980 nm) or $^4I_{9/2}$ (near 800 nm). Recently there has been an enormous interest by laser physicists and materials researchers in new upconversion processes and materials. Much of this research is oriented towards the development of visible and UV solid state lasers or phosphors which can be pumped by diode lasers in the near IR.[4]

Most of the systems studied so far, both glasses and crystals, are fluorides and oxides. They have the great advantage that they can be machined and handled in normal atmosphere. Chlorides, bromides, and iodides have received little attention. From a materials point of view they are not ideal, because they are more or less sensitive to moisture, and exposure to the atmosphere leads to their deterioration. From a purely scientific viewpoint, on the other hand, these heavier anion lattices are very interesting. Their lower phonon energies lead to a reduction of the multiphonon relaxation rates and thus to different excited state populations and dynamics. This was our main aim when we started this investigation of upconversion processes of lanthanide ions in heavy halide lattices.

Since one of the most important upconversion mechanisms is based on energy transfer between two excited ions in close proximity (see section 4.3 and ref 1), we have concentrated our effort on crystal lattices with close contacts between neighboring trivalent cations. One such structure is the so-called $RbDy_2Cl_7$-type structure, in which both $RbGd_2Cl_7$ and $RbGd_2Br_7$ crystallize.[5,6] The space group is *Pnma*, and there are two crystallographically nonequivalent Gd^{3+} ions in the unit cell.

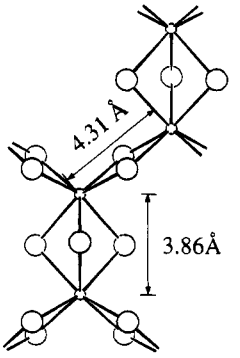

Figure 1. Bridging geometries and distances between nearest and next-nearest neighbor rare-earth ions within the layer structure of $RbGd_2Cl_7$.

The point symmetry of Gd^{3+} is C_s for both sites, and their coordination is 7-fold. As shown in Figure 1 the structure consists of dimer units with a short Gd^{3+}–Gd^{3+} distance of 3.86 Å in the chloride. These dimers are not isolated but interconnected to their four neighbor dimers in the b–c plane by relatively short bridges (4.31 Å). Thus the structure consists of strongly bonded $[Gd_2X_7]^-$ sheets staggered along [100] and connected by the Rb^+ ions. Due to the layer structure the crystals cleave very easily parallel to the (100) plane of the orthorhombic unit cell. Er^{3+} can be incorporated into these lattices, and Er^{3+} excitations below 31 000 cm^{-1} can be studied without any interference from the host lattice which has no absorptions in the visible and the near-UV. Er^{3+} ions are likely to replace Gd^{3+} ions in the doped crystals.

Here we present the results of high-resolution absorption and upconversion luminescence spectroscopy experiments of 1% Er^{3+}-doped $RbGd_2Cl_7$ and $RbGd_2Br_7$ crystals. The observations are rationalized using very simple and well-known concepts and models.

2. Experimental Section

Synthesis. Anhydrous ErX_3 and GdX_3 (X = Cl, Br) were prepared following the ammonium chloride route described in refs 7 and 8 and sublimed for purification. RbX was dried in a HX gas-flow. Sto-

[⊗] Abstract published in *Advance ACS Abstracts,* April 15, 1995.

(1) Auzel, F. E. *Proc. IEEE* **1973**, *61*, 758.
(2) Jacobsen, S. M.; Güdel, H. U. *J. Lumin.* **1989**, *43*, 125.
(3) Oetliker, U.; Riley, M. J.; May, P. S.; Güdel, H. U. *J. Lumin.* **1992**, *53*, 553.
(4) Lenth, W.; Facfarlane, R. M. *Opt. Photonic News* **1992**, *3*, 8.
(5) Meyer, G. *Z. Anorg. Allg. Chem.* **1982**, *491*, 217.
(6) Meyer, G.; Ax, P.; Cromm, A.; Linzmeier, H. *J. Less-Common Met.* **1984**, *98*, 323.
(7) Reed, J. B.; Hopkins, B. S.; Audrieth, L.F. *Inorg. Synth.* **1936**, *1*, 28.
(8) Meyer, G. *Inorg. Synth.* **1983**, *22*, 1.

0020-1669/95/1334-2745$09.00/0

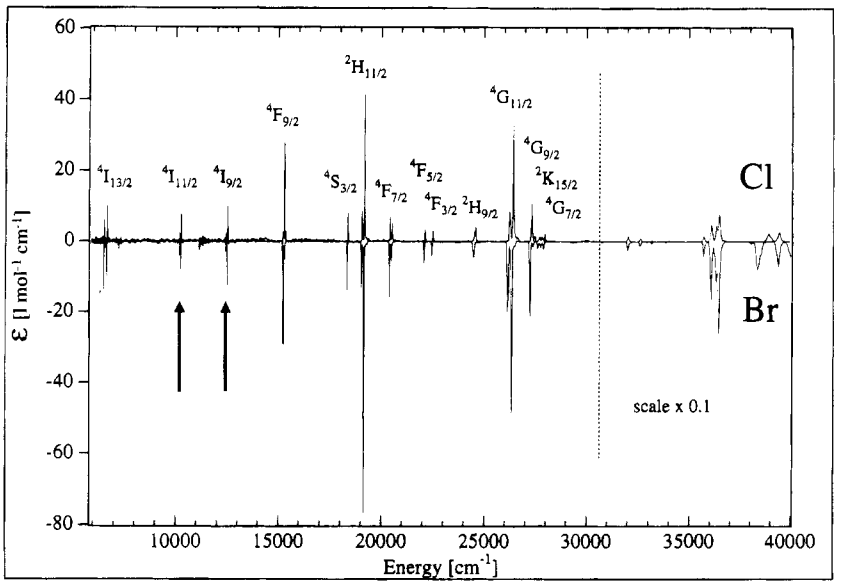

Figure 2. A survey of the crystal absorption spectra of $RbGd_2X_7$:1% Er^{3+} at 15 K. The two arrows indicate the excitation energies used for the upconversion experiments. The absorptions above 31 000 cm^{-1} are due to the host lattice. Note the corresponding scale change (broken line).

ichiometric amounts of RbX, ErX_3, and GdX_3 were sealed under vacuum in silica ampules, and the crystals were grown using the Bridgman technique. The crystals could be easily cleaved into plates. All handling was done under dry conditions in a glovebox due to the sensitivity of the substances to moisture.

Spectroscopy. All spectra were measured unpolarized with a random crystal orientation. The samples were enclosed in a copper cell or they were sealed into silica ampules, filled with 400 mbar helium gas for heat dissipation. Cooling was done with a closed-cycle cryostat (Air Products) for absorption, with a bath cryostat (Oxford Instruments MD4) or with a gas-flow technique for upconversion luminescence and Raman experiments.

The absorption spectra were recorded on a Cary 5e (Varian) spectrometer with typical instrumental resolutions of 5−10 and 1 Å for overview and detailed spectra, respectively.

For the upconversion luminescence spectra, the infrared excitation of the crystals was done with a multimode, standing wave Ti:sapphire laser (Schwartz Electro Optics), pumped by an argon-ion laser in all-lines mode (Spectra Physics 2045-15/4S). The laser beam was focused (f = 60 mm) onto the crystal. For excitation spectra, the wavelength control was achieved by an inchworm driven (Burleigh PZ-501) birefringent filter and a wavemeter (Burleigh WA2100). The sample luminescence was dispersed by a 0.85 m double monochromator (Spex 1402) with gratings blazed at 500 nm (1200 grooves/mm). The signal was detected with a cooled photomultiplier tube (RCA 31034) and a photon counting system (Stanford Research SR400). High luminescence intensities were attenuated with neutral density filters (Balzers). Device control and data acquisition were done by a personal computer. For the Raman measurements the randomly oriented crystals were excited with the 476.5 nm line of an argon-ion laser and checked with the 496.5 nm line for plasma lines.

The upconversion luminescence spectra were corrected for the wavelength dependence of the monochromator and detector sensitivity. No correction was applied to the excitation spectra covering only a small spectral range. The data were analyzed using Igor (Wave Metrics).

3. Results

The unpolarized crystal absorption spectra of $RbGd_2Cl_7$:1% Er^{3+} and $RbGd_2Br_7$:1% Er^{3+} at 15 K are reproduced in Figure 2. The absorptions above 31 000 cm^{-1} are due to $^8S_{7/2} \rightarrow {}^6P_J$ excitations of the Gd^{3+} host lattice. We only consider the Er^{3+} excitations below this energy. They are readily identified as f−f transitions within the $(4f)^{11}$ electron configuration on the basis of their energies and narrow line widths. The general assignment of the multiplets given in Figure 2 is straightforward from a comparison with the literature.[9,10] The multiplet energies in the bromide are seen to be slightly red-shifted with respect to the chloride. The two arrows in Figure 2 indicate the excitation energies used for the upconversion luminescence experiments.

Both title compounds show bright visible luminescence upon $^4I_{11/2}$ or $^4I_{9/2}$ excitation at all temperatures. Figure 3 shows room temperature upconversion luminescence spectra of the title compounds in the visible region after $^4I_{15/2} \rightarrow {}^4I_{11/2}$ excitation in the near-IR around 980 nm. The two spectra are distinctly different. The chloride spectrum is dominated by the green $^4S_{3/2}$ and $^2H_{11/2}$ luminescences, whereas in the bromide the blue-green $^4F_{7/2}$ luminescence accounts for more than 90% of the total intensity.

Figure 4 shows upconversion luminescence spectra between 5 and 295 K of $RbGd_2Cl_7$:1% Er^{3+} after $^4I_{15/2} \rightarrow {}^4I_{9/2}$ excitation around 800 nm. The overall upconversion intensity is highest at 77 K. Besides the visible luminescences two near-UV transitions are quite prominent. Three transitions originating from the high-energy excited state $^2H_{9/2}$ are recognized at all temperatures. At 5 K these $^2H_{9/2}$ luminescences dominate the upconversion spectrum, whereas at higher temperatures $^4S_{3/2}$ and $^2H_{11/2}$ become more important. In the bromide host the behavior is similar.

In Figure 5 the low-temperature absorption and upconversion luminescence lines are highly resolved and compared for the $^4I_{15/2} \leftrightarrow {}^4F_{9/2}$ transition. For both host lattices the common origins are easily identified. The overall appearance of the chloride and bromide spectra is very similar. The red-shift observed in Figure 2 is more clearly visible here as indicated by the arrow. A doubling of the lines due to the two Er^{3+} sites in the crystal is resolved in the chloride spectrum as indicated by the broken lines. The total energy splitting of the line multiplet is smaller by a few percent in the bromide than the chloride. From an analogous comparison of all the transitions, the baricenter energies and overall crystal-field splitting ranges listed in Table 1 were derived.

Figure 6 shows low-temperature Raman spectra of both host lattices. The highest energy vibrations are indicated with an

(9) Dieke, G. K.; Crosswhite, H. M. *Appl. Opt.* **1963**, *2*, 675.
(10) Richardson, F. S.; Reid, M. F.; Dallara, J. J.; Smith, R. D. *J. Chem. Phys.* **1985**, *83*, 3813.

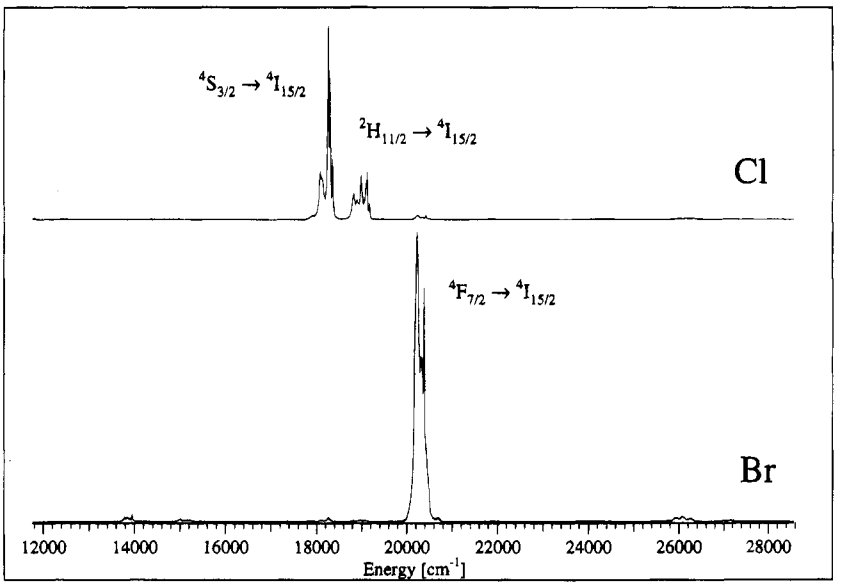

Figure 3. Room temperature upconversion luminescence spectra of $RbGd_2Cl_7$:1% Er^{3+} and $RbGd_2Br_7$:1% Er^{3+} with $^4I_{15/2} \rightarrow {}^4I_{11/2}$ excitation at 10 255 and 10 229 cm^{-1}, respectively.

Table 1. Baricenter Energies and Overall Crystal-Field Splittings in $RbGd_2X_7$:1% Er^{3+} [a]

	baricenter (cm^{-1})		splitting (cm^{-1})	
multiplet	Cl	Br	Cl	Br
$^4I_{15/2}$	129	120	260	230
$^4I_{13/2}$	6 607	6 586	169	145
$^4I_{11/2}$	10 228	10 218	75	64
$^4I_{9/2}$	12 461	12 438	163	145
$^4F_{9/2}$	15 274	15 246	146	138
$^4S_{3/2}$	18 357	18 325	43	41
$^2H_{11/2}$	19 119	19 073	141	131
$^4F_{7/2}$	20 496	20 450	107	105
$^4F_{5/2}$	22 158	22 095	50	50
$^4F_{3/2}$	22 497	22 450	45	41
$^2H_{9/2}$	24 517	24 460	115	105
$^4G_{11/2}$	26 309	26 219	209	201
$^4G_{9/2}$	27 381	27 290	208	201

[a] The data are derived from the high resolution absorption and luminescence spectra measured at cryogenic temperatures.

arrow. The peaks marked with asterisks are probably due to luminescence from impurities of other rare-earth ions.

4. Discussion

4.1. f−f Energy Levels. The labeling of the f−f transitions in Figure 2 is straightforward. The term to term energies are only very slightly dependent on the chemical coordination, and we can simply use the well-known diagram of Dieke to make an assignment of the well-separated multiplets.

The observed slight red-shift of the bromide energies with respect to those in the chloride host is a manifestation of an influence of the chemical bonding on the f−f excitation energies. We see it in Figures 2 and 5 as well as in Table 1. There are two principal effects leading to this red-shift. One is a reduction of the f-electron repulsion parameters with increasing covalency. This will lead to an energy reduction which more or less scales with the absolute excitation energies. In addition, the increasing covalency also reduces the spin−orbit splitting through an increase of the orbital reduction. Thus of all the ^4F_J terms the $^4F_{9/2}$ baricenter energies of the chloride and bromide are seen to be the most similar in Table 1. This is because the reduction in the Racah parameters affects all the ^4F_J terms in the same way, whereas the reduction in the spin−orbit splitting leads to a relative energy increase of $^4F_{9/2}$ with respect to the baricenter of the ^4F_J multiplets. A reduction of f−f multiplet energies along the halide series was noted in the very early days of lanthanide spectroscopy in PrX_3 and NdX_3 ($X = F^-$, Cl^-, Br^-, I^-).[11] Ephraim reported percentage red-shifts of 1.61−1.98 (F−Cl), 0.64−0.68 (Cl−Br) and 1.23−1.36 (Cl−I) in PrX_3. Our observed red-shifts for Er^{3+} are slightly smaller.

We have chosen the $^4I_{15/2} \leftrightarrow {}^4F_{9/2}$ transitions in Figure 5 to illustrate the effects of the crystal field. The overall splitting range in the luminescence spectrum is reduced from 260 to 230 cm^{-1} between the chloride and the bromide, and for the absorption lines the corresponding values are 146 and 138 cm^{-1}, respectively. All the absorption multiplets were thus analyzed and the corresponding numbers appear in the last column of Table 1. Depending on the multiplet under consideration the overall crystal-field splitting in the bromide host is reduced by a percentage between 0 and 15%. It is not possible to perform a quantitative analysis of the crystal field splitting for this host lattice. Such analyses have been performed for Er^{3+} in high-symmetry host lattices such as the cubic elpasolite Cs_2NaYCl_6[10] and the uniaxial host lattices $CsCdBr_3$[12] and $Cs_3Lu_2Br_9$.[13] In our host lattice the point group symmetry of Gd^{3+} is C_s and, as seen in Figure 1, the coordination number is sevenfold. In addition, there are two crystallographically nonequivalent Gd^{3+} sites in this lattice. The inequivalence is only very small, and we see its manifestation in the doubling of the absorption lines in the chloride lattice in Figure 5. In the bromide host the doubling remains unresolved for the high energy bands, as it does for most transitions in both lattices. Having no possibility to model the observed crystal field splitting we are thus left with an empirical discussion. In point symmetry C_s all the degeneracies are lifted and the electronic levels are Kramers doublets. The five levels resulting from $^4F_{9/2}$ are readily identified in the top trace of Figure 5 where the five doublets are indicated by broken lines. By analogy the corresponding splitting can be derived for the bromide. The eight levels of the $^4I_{15/2}$ ground state appear in two groups. There are five levels within the first 100 cm^{-1}, and after an energy gap of

(11) Ephraim, F.; Rây, P. *Ber. Dtsch. Chem. Ges.* **1929**, *62*, 1509 and references cited therein.
(12) Gruber, J. B.; Quagliano, J. R.; Reid, M. F.; Richardson, F. S.; Hills, M. E.; Seltzer, M. D.; Stevens, S. B.; Morrison, C. A.; Allik, T. H. *Phys. Rev. B* **1993**, *48*, 15561.
(13) Hehlen, M. P.; Güdel, H. U.; Quagliano, J. R. *J. Chem. Phys.*, in press.

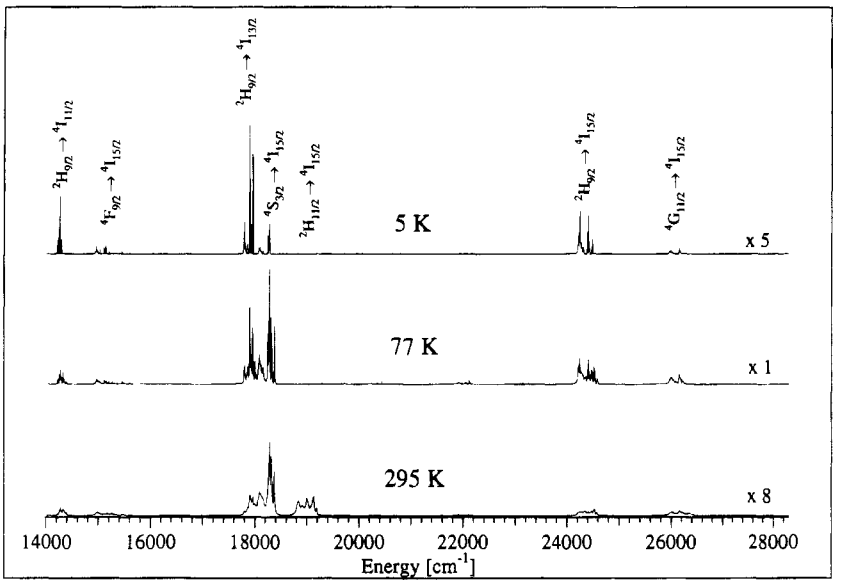

Figure 4. Visible and near-UV upconversion luminescence spectra of $RbGd_2Cl_7$:1% Er^{3+} excited into $^4I_{9/2}$ at 12 516, 12 520, and 12 520 cm^{-1} for 295, 77, and 5 K, respectively. Note the different intensity scales.

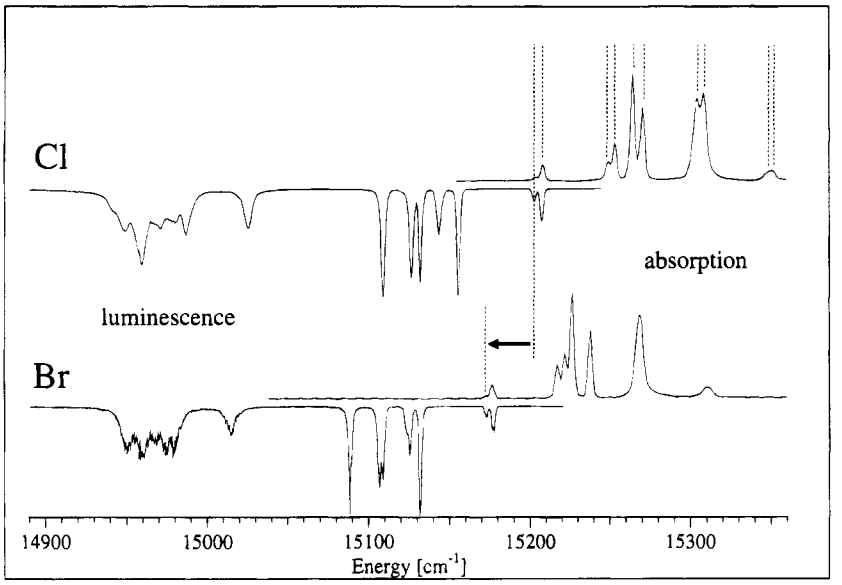

Figure 5. Crystal absorption (up, 15 K) and upconversion luminescence (down, 5 K) spectra of $RbGd_2X_7$:1% Er^{3+} in the region of $^4I_{15/2} \leftrightarrow {}^4F_{9/2}$ transitions. The redshift of the bromide spectrum is indicated by the arrow. The broken lines show the doublet structure of the absorption lines in the chloride.

70−80 cm^{-1}, three more levels are observed within 80 cm^{-1}. A similar pattern with two groups of five and three levels, respectively, was deduced for Er^{3+} in Cs_2NaYCl_6[10] with exactly octahedral coordination.

4.2. f−f Transition Intensities. If one aims at developing a new material for a solid-state laser or a phosphor a consideration of intensities and oscillator strengths is at least as important as the energetic part. Excited state dynamics in these systems are governed by a competition between radiative and nonradiative processes. Some of the latter will be discussed in section 4.4. The knowledge or at least an estimate of the radiative transition rate constants for the relevant luminescence transitions is therefore desirable. It is particularly important for an assessment of the laser potential, because the stimulated emission cross section is proportional to the oscillator strength. It has been shown in other host lattices that those transitions which are found to have the highest computed oscillator strengths do lase in upconversion pumping experiments.[14]

f−f transitions are parity forbidden in the free ion or in a centrosymmetric crystal environment. The lowest-energy odd-parity states which can act as a source of intensity in the case of Er^{3+} are 4f → 5d excitations. From our studies in Er^{3+}-doped $Cs_3Lu_2X_9$[15] and K_2LaX_5, in which there are no host lattice absorptions in the near-UV, we know that the lowest-energy 4f → 5d absorptions start at around 40 000 cm^{-1} in the bromide lattices, in the chloride lattices they cannot be seen up to 47 000 cm^{-1}. Since there is no center of inversion at the Er^{3+} site in the title compounds, there is a static crystal-field operator mixing f−f with f−d excitations.

Wavefunctions of very high quality are required to calculate intensities of f−f transitions including their distribution among the various crystal-field components. An example has recently been provided by a complete crystal-field analysis of Er^{3+}-doped $CsCdBr_3$.[12] For reasons discussed above, an analogous analysis is impossible for the present host lattices. We therefore have to resort to an approximation which only considers term to term intensities and makes use of the observed absorption intensities.

(14) McFarlane, R. A. *OSA Porc. Adv. Solid-State Lasers* **1992**, 275.
(15) Hehlen, M. P.; Krämer, K.; Güdel, H. U.; McFarlane, R. A.; Schwartz, R. N. *Phys. Rev. B* **1994**, *49*, 12475.

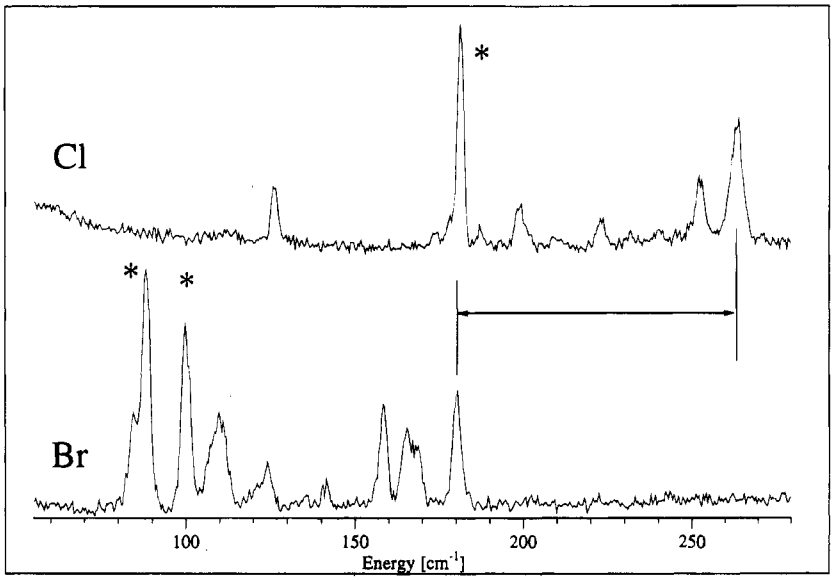

Figure 6. 10 K Raman spectra of the title compounds, excited at 476.5 nm. The arrow connects the highest-energy vibrations. The asterisks (*) indicate luminescence lines from impurities of other rare-earth ions.

This so-called Judd–Ofelt method is well established in the physical literature.[16,17] Instead of reproducing the derivation of the formalism here we refer to the book of Wybourne and simply write down the equation used for computing the intensities.[18] The oscillator strength of a term to term transition within an f^n electron configuration $|SLJ\rangle \rightarrow |S'L'J'\rangle$ is given by

$$f = \frac{8\pi m\nu}{3h} \frac{\chi}{(2J+1)} \sum_{\lambda=2,4,6} \Omega_{(\lambda)} |\langle f^n SLJ||U^{(\lambda)}||f^n S'L'J'\rangle|^2 \quad (1)$$

where χ is the local field correction, $\Omega_{(\lambda)}$ are the Judd–Ofelt intensity parameters, and the last factor is a reduced matrix element of the tensor operator $U^{(\lambda)}$. Physically this operator stands for the electron repulsion and the spin–orbit coupling. The reduced matrix elements are expressed in terms of the parameters $F_{(2)}$, $F_{(4)}$, $F_{(6)}$, and ζ which are pretty well-known for Er^{3+}.[13] In this simplified model the term to term intensities are thus expressed in terms of seven parameters. Four of these are taken from the literature, and the Judd–Ofelt parameters $\Omega_{(\lambda)}$ are determined from a least-square fit to the experimental absorption intensities.

We have performed such an analysis for the Er^{3+}-doped chloride host lattice and used the resulting parameters to predict the oscillator strengths of some relevant inter-excited-state transitions. The result is shown in Table 2. It is very similar in the bromide host. We notice that the 12 observed absorption intensities are well reproduced by the model with three adjustable parameters. On the other hand, the observed luminescence intensity branching ratios from the states $^2H_{9/2}$ (extracted from Figure 4) and $^4F_{7/2}$ (from Figure 3) deviate quite significantly from the calculated ones. The smaller the radiative rate constant, the larger the deviation. This is due to the fact that the Judd–Ofelt theory does not include nonradiative processes. For both $^2H_{9/2}$ and $^4F_{7/2}$ multiphonon relaxation processes compete with the luminescence, and the transitions with the smallest radiative rate constants are affected most.

According to an empirical rule successfully used in Er^{3+}-doped fluoride lattices,[14] an oscillator strength of at least 10^{-6} is necessary for a transition to be a potential laser transition.

Table 2. Experimental and Calculated Term to Term Oscillator Strengths f ($\times 10^{-6}$) and Emission Rate Constants k ($\times 10^3$ s^{-1}) Using eq 1 with the Following Parameter Values: $F_{(2)} = 96\,619$ cm^{-1}, $F_{(4)} = 67\,471$ cm^{-1}, $F_{(6)} = 48\,586$ cm^{-1}, and $\zeta = 2360$ cm^{-1} from ref 13 and $\Omega_{(2)} = 1.15972 \times 10^{-19}$ cm^{-1}, $\Omega_{(4)} = 2.98885 \times 10^{-20}$ cm^{-1}, and $\Omega_{(6)} = 9.53037 \times 10^{-21}$ cm^{-1}

absorption			emission			
transition	f_{obs}	f_{calc}	transition	f_{calc}	k_{calc}	k_{obs}[a]
$^4I_{15/2} \rightarrow {}^4I_{13/2}$	2.1	2.0	$^2H_{9/2} \rightarrow {}^4I_{15/2}$	1.5	2.0	0.57
$^4I_{11/2}$	0.8	0.9	$^4I_{13/2}$	4.1	2.9	2.9
$^4I_{9/2}$	0.8	0.8	$^4I_{11/2}$	2.1	1.0	0.14
$^4F_{9/2}$	3.1	3.5	$^4F_{7/2} \rightarrow {}^4I_{15/2}$	4.9	4.5	4.5
$^4S_{3/2}$	0.8	0.4	$^4I_{13/2}$	3.3	1.4	0.25
$^2H_{11/2}$	20.4	18.0	$^4I_{11/2}$	2.2	0.5	
$^4F_{7/2}$	2.3	2.4	$^4I_{9/2}$	1.7	0.2	
$^4F_{5/2}$	0.6	0.6	$^4F_{9/2}$	0.5	0.03	
$^4F_{3/2}$	0.4	0.4	$^2H_{11/2} \rightarrow {}^4I_{15/2}$	24.0	19.3	
$^2H_{9/2}$	1.0	0.9	$^4S_{3/2} \rightarrow {}^4I_{15/2}$	1.7	1.3	
$^4G_{11/2}$	41.3	42.3	$^4F_{9/2} \rightarrow {}^4I_{15/2}$	5.7	2.9	
$^4G_{9/2}$	3.2	2.6				

[a] The experimental emission data are scaled to the calculated value of the most intense branch.

We see in Table 2 that this is particularly true for $^4F_{7/2} \rightarrow {}^4I_{15/2}$. This transition has never been considered as a potential laser transition so far, because the $^4F_{7/2}$ is readily quenched by multiphonon relaxation processes in oxides, fluorides, and most chlorides. As will be shown in section 4.4, the situation is very different in bromides, and $^4F_{7/2} \rightarrow {}^4I_{15/2}$ thus becomes a candidate for laser action.

4.3. Upconversion and Cross-Relaxation. The observation of intense visible luminescence upon near-IR excitation is a clear manifestation of upconversion processes. Near-IR → vis upconversion is ubiquitous among Pr^{3+}-, Nd^{3+}-, Ho^{3+}-, Er^{3+}-, and Tm^{3+}-containing compounds. But the efficiency of the processes involved strongly depends on the structural and chemical characteristics of the compound. Most of the materials oriented studies have centered on oxide and fluoride lattices, which can be handled without any precautions in air. Most chloride, bromide, and iodide host lattices, on the other hand, are hygroscopic. As a consequence much less is known about the excited state dynamics in such systems.

There are a number of possible mechanisms for near-IR → vis upconversion in an Er^{3+} system.[1] The two most probable ones are as follows: (i) the sequential absorption of two photons

(16) Judd, B. R. *Phys. Rev.* **1962**, *127*, 750.
(17) Ofelt, G. F. *J. Chem. Phys.* **1962**, *37*, 511.
(18) Wybourne, B. G. *Spectroscopic Properties of Rare Earth*; Interscience Publishers: New York, 1995.

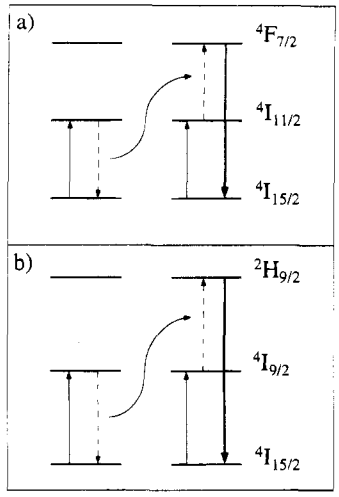

Figure 7. Schematic representation of energy-transfer upconversion processes in Er^{3+} systems.

by an Er^{3+} ion and (ii) excitation energy transfer between close-lying Er^{3+} ions in the lattice. We will abbreviate these processes ESA (excited state absorption) and ETU (energy transfer upconversion) respectively, in the following. In our host lattices the ETU mechanism is likely to play a dominant part because of the close proximity of nearest and next-nearest neighbors. We cannot, however, rule out contributions from the ESA process for some specific transitions. Time-resolved measurements are necessary to distinguish between the two.[19] In Figure 7 we have schematically drawn the diagrams for the two relevant ETU processes. Two excited Er^{3+} ions in close proximity are sharing their excitations to create a highly excited state on one of the ions. This can happen by both electric multipole or exchange mechanisms. For the nearest and second-nearest neighbor arrangements shown in Figure 1 an exchange mechanism is more likely. In a systematic study of exchange effects in dimer systems of the formula $Cs_3M_2X_9$ (M = Cr, Tb, Dy, Ho, Yb; X = Cl, Br) we have found relatively large exchange splittings resulting from the close proximity of the two M^{3+} ions. In our host lattice there is a very similar bridging geometry of the nearest neighbors. The fundamental difference between the two lattice types lies in the fact that in the present systems the dimers are connected in the $b-c$ plane with relatively short second-nearest neighbor distances of less than 5 Å; see Figure 1. Besides the binary halides MX_3 (25 mol % RE) the compounds AM_2X_7 (20 mol % RE) are those with the highest rare earth content. Due to this compact structure with short distances within the $b-c$ plane and also across the planes (shortest interplane distance 6.44 Å in $RbGd_2Cl_7$) ETU is expected to be important even at low doping levels. At 1% Er^{3+} concentration, assuming a statistical distribution, there is a 3% likelihood that a given Er^{3+} ion has an Er^{+} nearest or next-nearest neighbor (exchange interaction) and a 24.5% likelihood for at least one Er^{3+} neighbor within a radius of 10 Å (electric multipole mechanism). Energy transfer by an electric dipole mechanism between Er^{3+} ions at these distances can be very efficient.[19]

Er^{3+} offers a very favorable energy level scheme for upconversion. $^4F_{7/2}$ and $^2H_{9/2}$ lie almost exactly at twice the energy of $^4I_{11/2}$ and $^4I_{9/2}$, respectively. This is true as long as we neglect the crystal-field splittings of the states involved, as we have done so far. If we do consider these additional splittings we find that exact energy resonance is very rare, and

(19) Hehlen, M. P.; Frei, G.; Güdel, H. U. *Phys. Rev. B*, in press.

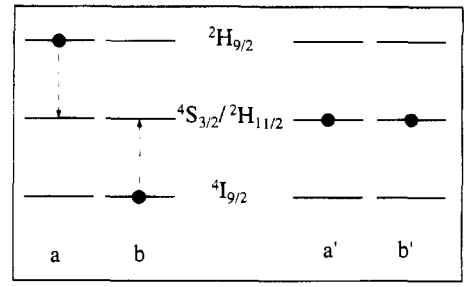

Figure 8. Schematic representation of a cross relaxation process in Er^{3+} systems after $^4I_{9/2}$ excitation and $^2H_{9/2}$ upconversion (Figure 7b).

usually there is a mismatch between a few and a few hundred wavenumbers.

The experimental results of our upconversion measurements show quite a different behavior for chloride and bromide upon $^4I_{11/2}$ excitation, see Figure 3. The bromide spectrum in Figure 3 conforms exactly to the upconversion scheme in Figure 7a, whereas the chloride spectrum resembles the upconversion spectra of Er^{3+}-doped fluoride or oxide host lattices. It appears that in all but the bromide lattice there are efficient nonradiative relaxation processes after the initial upconversion step. These will be discussed in the next section. The upconversion luminescence of $RbGd_2Br_7$:1% Er^{3+} after $^4I_{11/2}$ excitation is blue-green, distinctly different from the yellow-green of most chlorides and all fluorides and oxides. From a materials point of view this makes the bromide very attractive for potential applications.

For $^4I_{9/2}$ excitation the chloride (Figure 4) and bromide lattices exhibit very similar behavior. At 5 K the results are as expected from the simple mechanism of Figure 7b. Most of the luminescence intensity lies in the three transitions from $^2H_{9/2}$ to the three lowest-energy ^4I_J multiplets. The $^2H_{9/2} \rightarrow {}^4I_{13/2}$ transition is the most intense, and it is responsible for the strong yellow tint of the green luminescence. The intensity distribution among the various $^2H_{9/2} \rightarrow {}^4I_J$ transitions, i.e. the $^2H_{9/2}$ branching ratio was discussed in the previous section. With increasing temperature we see the $^4S_{3/2}$ and $^2H_{11/2}$ luminescences in the green spectral range come up in relative intensity. The most likely process to account for this obesrvation is schematically depicted in Figure 8. It is a cross-relaxation process involving two Er^{3+} ions in close proximity. Excitation energy is transferred from the highly excited Er^{3+} ion ($^2H_{9/2}$) to its partner in the lower excited state ($^4I_{9/2}$). Both $^4I_{9/2}$ and $^2H_{9/2}$ have relatively high populations under these experimental conditions, the former by direct laser excitation and the latter by the subsequent upconversion process. The cross-relaxation process is found to be thermally activated. Of the three possible processes $^2H_{9/2}/^4I_{9/2} \rightarrow {}^4S_{3/2}/^4S_{3/2}$ (1), $^4S_{3/2}/^2H_{11/2}$ (2), and $^2H_{11/2}/^2H_{11/2}$ (3) the first one releases an energy of 163 cm^{-1}, whereas the second and the third process require energies of 554 and 1271 cm^{-1}, respectively. We therefore conclude that either process (2) or (3) is operative in our case.

It is worth pointing out that a process of the type shown in Figure 8 is physically very similar to the ETU upconversion process discussed earlier. If we take the reverse process in Figure 8, i.e. from right to left, we would talk about an upconversion process. Both the upconversion and the cross-relaxation processes are governed by the same matrix elements, and in which direction the reaction proceeds only depends in the initial populations. In our case the conditions are such that $^4I_{9/2}$ and $^2H_{9/2}$ populations are continuously created by laser excitation so that the reaction in Figure 8 proceeds from left to right. On the basis of the same reasoning, the upconversion processes in Figure 7 are much more likely than the reverse

cross-relaxations under continuous laser excitation in the near-IR. Other mechanisms to populate the $^4S_{3/2}$ and $^2H_{11/2}$ states are the cross-relaxation $^4I_{9/2}/^4I_{13/2} \rightarrow {}^4S_{3/2}/^4I_{15/2}$ or a $^4I_{13/2} \rightarrow {}^2H_{11/2}$ excited state absorption.

At 295 K in Figure 4 there is a relatively intense $^2H_{11/2}$ luminescence. We attribute this to a thermal population of the $^2H_{11/2}$ from $^4S_{3/2}$. The energy difference between $^4S_{3/2}$ and the lowest $^2H_{11/2}$ level is 674 and 664 cm^{-1} for the chloride and bromide, respectively. We can thus expect 7% $^2H_{11/2}$ population at most at 295 K. But the total oscillator strength of $^4I_{15/2} \leftrightarrow {}^2H_{11/2}$ is 24 times bigger than for $^4I_{15/2} \leftrightarrow {}^4S_{3/2}$, Figure 2 and Table 2, resulting in comparable intensities for the two transitions at 295 K.

In both Figures 3 and 4 we notice some $^4G_{11/2}$ luminescence in the near-UV around 26 000 cm^{-1}. It is clear that at least three near-IR photons are needed to get up to this high energy. At this point any idea about the possible combinations of upconversion and cross-relaxation mechanisms to obtain $^4G_{11/2}$ population would be speculative.

4.4. Multiphonon Relaxation. The most striking and most interesting result of this study is the completely different behavior of $RbGd_2Br_7$:1% Er^{3+} after $^4I_{11/2}$ excitation, Figure 3. It is different not only to the corresponding chloride but also to the fluorides and oxides reported in the literature. On the other hand, similar behavior has been observed in other bromides such as $Cs_3Lu_2Br_9$,[15] $CsCdBr_3$,[20] and K_2LaBr_5.[21] At first sight this is surprising, since Figure 2 and Table 1 clearly show that the spectroscopic properties of Er^{3+}-doped $RbGd_2Cl_7$ and $RbGd_2Br_7$ are very similar indeed. In section 4.1 we noted differences of the relevant electronic parameters of the order of a few percent between chloride and bromide. Clearly, these cannot be responsible for the observed differences in Figure 3. Rather, we have to consider the vibrational properties of the two lattices and their consequences.

The Raman spectra reproduced in Figure 6 show how the energy of the highest-energy vibration decreases from 264 cm^{-1} in $RbGd_2Cl_7$ to 180 cm^{-1} in $RbGd_2Br_7$. This is essentially the breathing vibration of the GdX_7 or ErX_7 polyhedron. Nonradiative processes in which electronic energy is converted into vibrational energy, so-called multiphonon relaxation processes, are known to depend very critically on the electronic energy gap and on the vibrational frequency of the active vibrations in the process, the so-called accepting modes. In Er^{3+}-doped $RbGd_2Cl_7$ and $RbGd_2Br_7$ the energy gaps are very similar, but the phonon energies are significantly different. We suspect that this is the reason for the observed difference in Figure 3, and we proceed to a semiquantitative analysis.

The experimental $^4F_{7/2}$ luminescence lifetimes at 295 K are 6 and 110 μs for the chloride and bromide, respectively. To distinguish between the radiative and nonradiative fraction, we use the spectrum in Figure 3. On the basis of the assumption that the multiphonon relaxation of the $^4F_{7/2}$ state is reflected by the $^4S_{3/2}/^2H_{11/2}$ luminescence intensity (cf. Figure 9) this ratio is readily determined. Furthermore, multiphonon relaxation from $^4S_{3/2}/^2H_{11/2}$ is neglected due to the large energy gap to the next lower state. The resulting ratio of radiative to non-radiative rate constants is approximately 1:40 and 60:1 for the chloride and bromide, respectively. The numbers are collected in Table 3. First we notice that the k_{rad} values for the chloride and bromide are similar as expected. Summing up the rate constants of the various $^4F_{7/2}$ transitions from the Judd–Ofelt analysis we get a theoretical $k_{rad} = 6735\ s^{-1}$. Considering the approximative nature of the Judd–Ofelt technique the agreement with experiment is good.

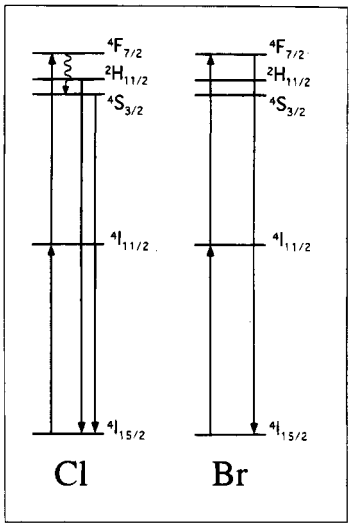

Figure 9. Schematic representation of the multiphonon relaxation in $RbGd_2Cl_7$:1% Er^{3+} (left) and the radiative transition in $RbGd_2Br_7$:1% Er^{3+} (right) after $^4F_{7/2}$ excitation.

Table 3. Experimental Rate Constants ($\times 10^3\ s^{-1}$) for Radiative and Multiphonon $^4F_{7/2}$ Decay

	$k_{tot.}$	k_{rad}	k_{mp}
Cl	167	4	163
Br	9.1	8.9	0.15

Considering now the nonradiative part of the $^4F_{7/2}$ relaxation, which is essential for our discussion, we get an experimental ratio Cl/Br of about three orders of magnitude. This value can be compared with the value derived from the normalized energy gap law,[22] which is often applied in such situations:

$$k_{mp} = \beta e^{-\alpha(\Delta E/\hbar\omega)} \qquad (2)$$

In eq 2 α and β are host dependent constants, ΔE is the electronic energy gap, and $\hbar\omega$ is the energy of the accepting vibrational mode. According to this equation the highest-energy phonons will be the most effective accepting modes. The relevant gap in our case is between the lowest crystal-field level of $^4F_{7/2}$ and the highest level of $^2H_{11/2}$. From the high-resolution absorption spectra we deduce values of 1242 and 1247 cm^{-1} for the chloride and bromide, respectively. With the phonon energies of 264 cm^{-1} (Cl) and 180 cm^{-1} (Br) we get a reduced energy gap of 4.7 and 6.9 phonons for the chloride and bromide, respectively. Assuming now $\beta_{Cl} \approx \beta_{Br}$, $\alpha_{Cl} \approx \alpha_{Br} = \alpha$ and using eq 2 with the above experimental ratio, we obtain an estimate for $\alpha = 3.1$. In the literature[23] we find α values of 3.8 and 3.5 for rare-earth ions in $LaCl_3$ and $LaBr_3$, respectively, reasonably close to our estimate.

From the numbers in Table 3 we finally arrive at the following important conclusion. It is not only the drastic reduction in k_{mp} which makes the bromide and the chloride behave so different. It is also the fact that the radiative relaxation rate constant of $^4F_{7/2}$ lies exactly in between the nonradiative rate constants of the chloride and the bromide which is necessary for this surprising switch of luminescence behavior. In the chloride we thus have $k_{mp} \gg k_{rad}$ and in the bromide $k_{mp} \ll k_{rad}$.

(20) Cockroft, N. G.; Jones, G. D.; Syme, R. W. G. *J. Lumin.* **1989**, *43*, 275.
(21) Krämer, K.; Güdel, H. U. *J. Alloys and Compd.* **1994**, *207/208*, 128.
(22) Riseberg, L. A.; Moos, H. W. *Phys. Rev.* **1968**, *174*, 429.
(23) van Dijk, J. M. F.; Schuurmans, M. F. H. *J. Chem. Phys.* **1983**, *78*, 5317.

5. Conclusions

By studying the spectroscopic properties of Er^{3+} in the isostructural host lattices $RbGd_2Cl_7$ and $RbGd_2Br_7$, we can follow and interpret the effect of a chemical variation on the photophysical properties which is quite dramatic. Unlike most of the host lattices investigated so far, Er^{3+}-doped $RbGd_2Br_7$ shows pure $^4F_{7/2}$ upconversion luminescence upon $^4I_{11/2}$ excitation at all temperatures between 5 and 295 K. Besides the fundamental scientific aspect, which has been discussed above, this raises some interesting possibilities for laser materials research.

A material with a luminescence wavelength below 500 nm which can be pumped in the near-IR with a diode laser is of considerable interest. The $^4S_{3/2}$ upconversion luminescence exhibited by oxide, fluoride, and most chloride host lattices lies close to 533 nm, where a doubled diode pumped Nd^{3+} laser is very competitive. In most of the Er^{3+} upconversion lasers reported so far the $^4S_{3/2} \rightarrow {}^4I_{15/2}$ transition is a laser transition. It would appear therefore, that host lattices with low phonon energies could open the way to shorter wavelength near-IR $\rightarrow$ vis upconversion laser or phosphor materials. These soft materials are usually not stable in air. So they have to be protected. In addition, it is not known whether their thermal conductivities are adequate for laser applications. With respect to materials sciences there are lots of open questions. This is an open field for research and development. The present study demonstrates that there is a potential here. As inorganic chemists we have probably more inclination to explore this area than more physically oriented scientists, because we are often more familiar with principles such as chemical or structural variation to tune physical or chemical properties. But when we come to the point of actually implementing a laser, we need the collaboration with laser physicists and engineers.

The host lattices described in this paper are not likely to ever be used as laser hosts. As a result of the close proximity of the nearest and next-nearest neighbors, Er^{3+}-doped $RbGd_2Cl_7$ and $RbGd_2Br_7$ are very efficient near-IR $\rightarrow$ vis upconverters. The crystals suffer from a very pronounced cleavage tendency parallel to the (100) plane which is detrimental for their optical properties. However, the lattices have served to demonstrate a few important phenomena and principles, and we feel that some more research is quite promising.

Acknowledgment. We thank M. Hehlen for providing his Judd–Ofelt program. Financial support by the Swiss National Science Foundation and by a grant from the priority program "Optics" administered by the Board of Swiss Federal Institutes of Technology is gratefully acknowledged.

IC950054N